Applied Mathematical Modelling 36 (2012) 6061–6071

Contents lists available at SciVerse ScienceDirect

Applied Mathematical Modelling

journal homepage: www.elsevier.com/locate/apm

Comparison of computations of asymptotic flow models in a constricted channel

F. Chouly [a], P.-Y. Lagrée [b,*]

[a] Laboratoire de Mathématiques de Besançon, CNRS UMR 6623, Université de Franche-Comté, 16 route de Gray, 25030 Besançon Cedex, France
[b] CNRS & UPMC Univ Paris 06, UMR 7190, Institut Jean Le Rond d'Alembert, Boîte 162, F-75005 Paris, France

ARTICLE INFO

Article history:
Received 15 March 2010
Received in revised form 12 January 2012
Accepted 17 January 2012
Available online 31 January 2012

Keywords:
Triple Deck
Double Deck
Boundary layer

ABSTRACT

We aim at comparing computations with asymptotic models issued from incompressible Navier–Stokes at high Reynolds number: the Reduced Navier–Stokes/Prandtl (RNS/P) equations and the Double Deck (DD) equations. We treat the case of the steady two dimensional flow in a constricted pipe. In particular, finite differences and finite element solvers are compared for the RNS/P equations. It results from this study that the two codes compare well. Numerical examples also illustrate the interest of these asymptotic models as well as the flexibility of the finite element solver.

1. Introduction

The 2D flow between parallel plates (or as well in a symmetrical pipe) with a constriction mimics a lot of flows of interest, among them one may think of blood flow in a stenosis [1–3], respiratory flow [4–6], pipes in the gas or oil industry [7]. Those kind of simplifications arising in the Saint–Venant equations as well (even if here we do not deal with moving interfaces). Of course, this problem may be considered as very classical with no more numerical difficulties. It may be solved by various numerical methods for the Navier–Stokes equations [8–11].

Therefore, we will focus on model equations issued from Navier–Stokes, when a long wave approximation may be done. Those equations are obtained by change of scales using the dominant balance principle to pick up the dominant terms [12]. The vanishing small terms are then removed from the complete set of Navier–Stokes equations. This approach is known since Prandtl pioneering work in 1905 [13,14] and several books now deal with asymptotic flow models [15–19].

The obtained equations are the Prandtl equations with different boundary conditions. So, one of the major difficulties is that those equations are not standard compared to Navier–Stokes or Euler equations, for which a huge variety of numerical methods have been developed. As a result, most of the numerical methods designed for Navier–Stokes fail to solve these equations, which in general present a parabolic character, and well-suited methods are not so much developed [20,17,21].

So, we will present in the first part Section 2 some asymptotic models issued from the Navier–Stokes equations. Those are the so called Reduced Navier–Stokes/Prandtl (RNS/P) [22] and the Double Deck (DD [23]) equations. In the second part Section 3, we will describe three numerical techniques that have been developed for these equations and that will be compared. The first is a finite difference method inspired from the classical procedures to solve parabolic equations, such as the heat equation [24, Ch. 6]. It has been developed and used in various contexts [22,25–28]. The second one is the "Keller Box" technique, which is also a finite difference method [20,29]. The last one is a finite element method, which main features are a low order approximation of the pressure and/or a grad–div stabilization term. It has been developed more recently [30] and for

* Corresponding author.
E-mail addresses: franz.chouly@univ-fcomte.fr (F. Chouly), pierre-yves.lagree@upmc.fr (P.-Y. Lagrée).
URLs: http://lmb.univ-fcomte.fr/franz-chouly (F. Chouly), http://www.lmm.jussieu.fr/~lagree (P.-Y. Lagrée).

0307-904X/$ - see front matter © 2012 Elsevier Inc. All rights reserved.
doi:10.1016/j.apm.2012.01.035

this reason needs to be validated through comparison with existing solutions or reference codes. Therefore, in a third part Section 4, we present numerical comparisons of those approaches. Furthermore, we confront simulations with the simplified model equations (RNS/P, DD) to simulations with the full Navier–Stokes equations. In Section 5, we finally draw conclusions about the numerical experiments and discuss the interest of both these models and methods. Concerning the skin friction and the pressure distribution at the wall, we will show that the results are similar, validating the models and the methods.

2. Mathematical flow models

2.1. Geometry and hypotheses

We want to compute the velocity and pressure field in a geometry like those of Fig. 1. It consists in two parallel plates with a symmetrical indentation. Note that the axi-symmetrical case is exactly the same in principle. The flow is supposed newtonian, laminar, incompressible and steady. It mainly goes from the inlet to the outlet. The base flow in the case of no indentation is the Poiseuille flow. We use the height h as scale and the velocity scale U_0 is such that the non dimensional Poiseuille flow reads

$$u(0,y) = (1-y)y, \ \ v = 0.$$

The Reynolds number is defined with h, U_0 and ν the constant viscosity: $Re = \frac{U_0 h}{\nu}$. It is supposed very large, but the flow is supposed to remain laminar.

The asymptotic models issued from high Reynolds number Navier–Stokes (NS) are the Reduced Navier–Stokes/Prandtl (RNS/P) equations and the Double Deck (DD) equations.

2.2. Navier–Stokes equations

The problem is to solve the Navier–Stokes equations written without dimensions:

$$\begin{cases} u\dfrac{\partial u}{\partial x} + v\dfrac{\partial u}{\partial y} = -\dfrac{\partial p}{\partial x} + \dfrac{1}{Re}\left(\dfrac{\partial^2 u}{\partial x^2} + \dfrac{\partial^2 u}{\partial y^2}\right), \\ u\dfrac{\partial v}{\partial x} + v\dfrac{\partial v}{\partial y} = -\dfrac{\partial p}{\partial y} + \dfrac{1}{Re}\left(\dfrac{\partial^2 v}{\partial x^2} + \dfrac{\partial^2 v}{\partial y^2}\right), \\ \dfrac{\partial u}{\partial x} + \dfrac{\partial v}{\partial y} = 0. \end{cases} \tag{1}$$

The boundary conditions are no-slip condition on the walls, a condition of symmetry, the initial velocity profile and the value of the pressure at the outlet:

$$u = v = 0 \text{ on } y = y_w(x), \ \frac{\partial u}{\partial y} = 0, \ \ v = 0 \text{ on } y = \frac{1}{2}, \ u(0,y) = (1-y)y \text{ and } p(x_{out}, y) = 0. \tag{2}$$

2.3. RNS/P

Looking at long bumps of scale L_b, with $L_b \gg h$, we may expand Navier–Stokes using this longitudinal scale and keeping transversally the h scale. So, using $x^* = L_b x$, $y^* = hy$, $u^* = U_0 u$, $v^* = V_0 v$ and $p^* = p_0 + \rho U_0^2 p$, we obtain a specific case when $L_b = hRe$ and $V_0 = U_0/Re$. With those scales, we obtain in fact the Prandtl equations. It means that the second order derivative term in x in the equations disappears because it is of order Re^{-2} and the pressure remains constant across the section because the transverse pressure gradient is of order Re^{-2}. We now formally write back in the scales $x^* = hx$, $y^* = hy$, $u^* = U_0 u$, $v^* = U_0 v$ this system and we obtain:

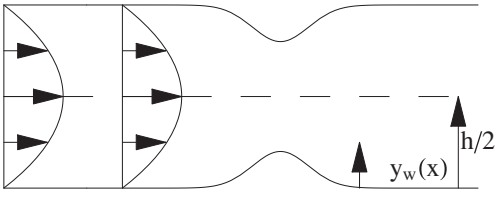

Fig. 1. The incompressible 2D flow between two plates, the lower plate is in $y = 0$, the upper in $y = h$. A symmetrical indentation is given at the lower wall as $y = y_w(x)$ and at the upper wall as $y = h - y_w(x)$. As the problem is symmetrical it is solved between $y_w(x)$ and $h/2$.

$$\begin{cases} u\dfrac{\partial u}{\partial x}+v\dfrac{\partial u}{\partial y}=-\dfrac{\partial p}{\partial x}+\dfrac{1}{Re}\dfrac{\partial^2 u}{\partial y^2}, \\ 0=-\dfrac{\partial p}{\partial y}, \\ \dfrac{\partial u}{\partial x}+\dfrac{\partial v}{\partial y}=0. \end{cases} \tag{3}$$

The boundary conditions are the no-slip condition on the wall, conditions of symmetry for the velocity field, the initial velocity profile and the value of the pressure at the inlet:

$$u=v=0 \text{ on } y=y_w(x),\ \frac{\partial u}{\partial y}=0,\ v=0 \text{ on } y=\frac{1}{2},\ u(0,y)=(1-y)y \text{ and a given } p(x_{in},y). \tag{4}$$

Note first that the total pressure drop $p(x_{in},y)-p(x_{out},y)$ is a result of the computation, so thereafter we use the output pressure as reference of pressure $p(x_{out},y)=0$. This is in general not the case in standard boundary layer theory [15] where the pressure is a given function. Note also that if we add the missing second order derivative $\frac{1}{Re}\frac{\partial^2 u}{\partial x^2}$ in $(3)_1$, the equations we obtain are the so called primitive equations used in oceanography [31].

2.4. Double Deck

2.4.1. Equations

Looking at small symmetrical bumps of scale ε, with $\varepsilon \ll 1$, in a Poiseuille flow, the basic profile is perturbed by the bumps. The core flow is unchanged, whereas the flow near the wall is dramatically changed leading eventually to flow separation. We may expand Navier–Stokes using this transversal scale ε and using longitudinally any L scale (consistant with the bump length). So, using $x^*=Lx,\ y^*=\varepsilon h y,\ u^*=\varepsilon U_0 u,\ v^*=(\varepsilon^2 h/L)U_0 v$ and $p^*=p_0+\rho\varepsilon^2 U_0^2 p$, we obtain a specific case (where transverse viscous effects and nonlinear effects have the same order of magnitude by dominant balance) when $\varepsilon=(L/h)^{1/3}Re^{-1/3}$. With those scales, we obtain in fact the Prandtl equations, but they are at a different scales and with different boundary conditions. They represent the perturbation induced by the bump near the wall in a layer called the "Lower Deck". The "Main Deck" is the core flow which remains unperturbed. Those equations are thus called the Double Deck equations [23] (much more asymptotic models linked to Double or Triple Deck may be constructed in pipe flows, see for example [25]).

In the Lower Deck:

$$\begin{cases} u\dfrac{\partial u}{\partial x}+v\dfrac{\partial u}{\partial y}=-\dfrac{\partial p}{\partial x}+\dfrac{\partial^2 u}{\partial y^2}, \\ 0=-\dfrac{\partial p}{\partial y}, \\ \dfrac{\partial u}{\partial x}+\dfrac{\partial v}{\partial y}=0. \end{cases} \tag{5}$$

The boundary conditions are no-slip condition at the wall, the initial linear velocity profile far upstream (which is the Poiseuille initial profile written near the wall) and the matching condition at infinity (which means that the core flow is not affected by the perturbation caused by the small bump):

$$u=v=0 \text{ on } y=y_w,\ u\to y \text{ when } x\to-\infty, \text{ and } u\to y \text{ when } y\to\infty. \tag{6}$$

Exactly the same set of equations may be written near the upper wall. The axis y being upside down. In the core flow (the Main-Deck) there is no perturbation.

2.4.2. Remark: the linear solution

We note that in this case we have a simple analytical solution in Fourier space obtained by linearisation [23], with TF and TF^{-1} the direct and reverse Fourier transforms:

$$\tau=U_0'+U_0'(3Ai(0))(U_0')^{1/3}TF^{-1}[(-ik)^{1/3}TF[y_w]] \tag{7}$$

$$p=(U_0')^2(3Ai'(0))(U_0')^{-1/3}TF^{-1}[(-ik)^{-1/3}TF[y_w]]. \tag{8}$$

where $Ai(x)$ is the Airy function, $Ai(0)=0.355028$ and $Ai'(0)=-0.258819$, with $U_0'=1$ the value of the slope velocity at the wall.

2.4.3. Remark: transverse pressure gradient

Just to explain some features of the non symmetrical case, we recall here that in the non symmetrical case there is a transverse pressure gradient in the Main Deck. This is the case for example when no bump is present on the upper wall. This transverse pressure gradient is due to the displacement of the stream lines and we obtain that the length of the bump must

be $hRe^{1/7}$ and then $\varepsilon = Re^{-2/7}$. Hence in the Main Deck, we introduce the classical displacement function $-A$ of the streamlines [23], then the transverse momentum equation issued from (1):

$$U_0(y)\frac{\partial v_1}{\partial x} = -\frac{\partial p_1}{\partial y}. \tag{9}$$

so that as $v_1 = -A'(x)U_0(y)$ and $p = Re^{-2/7}p_1$, the velocity is $u = U_0(y) + Re^{-2/7}A(x)U_0'(y)$ and $v = -Re^{-3/7}A'(x)U_0(y)$, so across the channel there is a pressure drop:

$$p_1(x,1) - p_1(x,0) = -A''(x)\int_0^1 U_0^2(y)dy, \tag{10}$$

and two systems of equations like (5) interact: a first one near the lower wall, but the matching condition at infinity is changed as: $u \to y + A$ when $y \to \infty$ and the pressure is $p = p_1(x,0)$ in the layer near the lower wall. The upper layer near the upper wall (with $y^* = h - \varepsilon h y$) has again equations like (5), but the matching condition at infinity is changed as: $u \to y - A$ when $y \to \infty$. The pressure is $p = p_1(x,1)$ in this layer. The symmetrical case corresponds to $A = 0$ which means that there is no displacement of the stream lines in the Main Deck.

3. Numerical methods

The presented methods aim at solving the RNS/P equations. Note however that they are also appropriate for the DD equations, through a change of boundary conditions (4) and (6).

3.1. Finite differences

The baseline of this finite differences method is to solve the problem (3) as a heat equation $u\frac{\partial u}{\partial x} + \cdots = \frac{\partial^2 u}{\partial y^2} + \cdots$ as the problem is a kind of heat equation, a marching procedure in x seems natural (like time-marching for the heat equation). The system is indeed parabolic, whereas steady Navier–Stokes equation present generally either an elliptic (at low Reynolds) or hyperbolic (at high Reynolds) character. Knowing the solution $u_{i,j}$ at station $x = i\Delta x$ for all transverse positions $y = j\Delta y$, the solution $u_{i+1,j}$ at next station $x = (i\Delta x) + \Delta x$ is to be found for all j. The second order derivative is implicited, a first guess for the pressure is $p^e_{i+1} = p_i$ and the previous step transverse velocity ($v_{i,j}$) is used. We have a tridiagonal system to solve which is done by Thomas algorithm [32]. This gives an estimation of the velocity $u^e_{i+1,j}$. From this estimation the incompressibility is solved by simple Euler integration in j starting from $v^e_{i+1,j=0} = 0$. Then $v^e_{i+1,j}$ is obtained. But, this velocity does not satisfy the symmetry condition for transverse velocity in $y = 1/2$. So we have to iterate on the value of the pressure p^e_{i+1} (by a Newton algorithm) in order to have a zero velocity at the upper side of the grid. The procedure breaks down if there is reverse flow. Nevertheless, we are able to compute reverse flow cases when $u < 0$ by putting $u^{ij} = 0$, this is known as the FLARE algorithm [33]. This method has been used in [22,25–28]. The same technique is used for the RNSP and the DD cases, only the boundary condition is changed.

3.2. Keller Box

The problem (3) can be solved using "Keller Box" technique (see e.g. [29] or [20]). This is also a finite differences marching scheme. The equations are written in introducing only first order derivatives:

$$\frac{\partial u}{\partial y} = G, \quad \frac{\partial G}{\partial y} = u\frac{\partial u}{\partial x} + \cdots$$

then, the derivatives are centered in the "box" of corners $(i-1,j-1)$ $(i-1,j)$ $(i,j-1)$ and (i,j). The values in $(i-1,j-1)$ $(i-1,j)$ are known. For example $\frac{\partial u}{\partial y} = G$, reads $\frac{u(i,j)-u(i,j-1)}{\Delta y} = \frac{G(i,j)+G(i,j-1)}{2}$. In fact we need four variables, ψ the stream function, G the shear and W a fictitious variable such that $\frac{\partial p}{\partial x} = -\frac{\partial (W^2/2)}{\partial x}$ (denoted as *Mechoul* approach by Cebeci & Keller) so that Prandtl equations are:

$$\begin{cases} \dfrac{\partial \psi}{\partial y} = u, \dfrac{\partial u}{\partial y} = G, \\ \dfrac{\partial G}{\partial y} = -\dfrac{\partial (W^2/2)}{\partial x} + u\dfrac{\partial u}{\partial x} - G\dfrac{\partial \psi}{\partial x}, \quad \dfrac{\partial W}{\partial y} = 0. \end{cases} \tag{11}$$

As among others there are non linear terms, so $u\frac{\partial u}{\partial x}$ is discretized in

$$\frac{\left(\dfrac{u(i,j)+u(i-1,j)}{2} + \dfrac{u(i,j-1)+u(i,j-1)}{2}\right)}{2}\frac{\left(\dfrac{u(i,j)-u(i-1,j)}{\Delta x} + \dfrac{u(i,j-1)-u(i-1,j-1)}{\Delta x}\right)}{2},$$

and then a Newton iteration is necessary. Writing the new step $n+1$ as a small increase of the preceding: $u^{n+1}(i,j) = u^n(i,j) + \delta u^n(i,j)$, we obtain a block tridiagonal system: $\delta u^n(i,j)$, $\delta G^n(i,j)$ *etc.* are solved by Thomas algorithm [32].

Boundary condition at the wall and at the entrance are simple. In the case of Double Deck (DD), at the top of the domain the velocity is equal to y so that the third equation of the system (11) becomes $0 = -\frac{\partial(W^2/2)}{\partial x} + u\frac{\partial u}{\partial x} - \frac{\partial \psi}{\partial x}$. Its integral $-W^2 + u^2 - 2\psi$ is then a constant at the top of the domain. This last expression is linearised to obtain the relation in $j = J$ (at the upper boundary):

$$J\Delta y \delta u^n(i,J) - \delta\psi^n(i,J) - W^n(i,J)\delta W^n(i,J) = 0.$$

A last important trick is to introduce again the so called FLARE (introduced in [33]) approximation: $u\frac{\partial u}{\partial x}$ is put to 0 when $u < 0$.

3.3. Finite elements

Finally, the system (3) can also be solved with a finite element method, the main features of which are similar to mixed methods for the incompressible Navier–Stokes equation. The adaptation of such methods is however not straightforward and requires an appropriate choice of finite element spaces/stabilization terms. The method described here has been proposed and analyzed in [30]. We call Ω the domain in which the equations are solved; Ω is supposed to be a polygonal domain in $\mathbb{R}^2$, with boundary $\partial\Omega$; $\Gamma_i \subset \partial\Omega$ is the entry (inlet flow), $\Gamma_w \subset \partial\Omega$ is the rigid wall with no-slip boundary conditions (case of the RNS/P equations) and $\Gamma_o \subset \partial\Omega$ is the exit (outlet flow). Let $\mathbf{H_h}$ be the finite element discretization space for the velocity and Π_h be the finite element space for the pressure. The discrete variational problem reads: *Find* $(u, v, p) \in \mathbf{H_h} \times \Pi_h$, $u = u^0$ *on* Γ_i, $u = 0$, $v = 0$ *on* Γ_w *such that:*

$$\begin{cases} \int_\Omega \left(u\frac{\partial u}{\partial x} + v\frac{\partial u}{\partial y}\right)\zeta + \frac{1}{Re}\int_\Omega \frac{\partial u}{\partial y}\frac{\partial \zeta}{\partial y} + \int_\Omega \lambda\left(\frac{\partial u}{\partial x} + \frac{\partial v}{\partial y}\right)\left(\frac{\partial \zeta}{\partial x} + \frac{\partial \xi}{\partial y}\right) \\ -\int_\Omega p\left(\frac{\partial \zeta}{\partial x} + \frac{\partial \xi}{\partial y}\right) + \int_\Omega q\left(\frac{\partial u}{\partial x} + \frac{\partial v}{\partial y}\right) = 0, \end{cases} \tag{12}$$

for all $(\zeta, \xi, q) \in \mathbf{H_h^0} \times \Pi_h$.

$\mathbf{H_h^0}$ is the subspace of $\mathbf{H_h}$ with functions of vanishing trace on $\Gamma_i \cup \Gamma_w$. A continuation strategy which consists in increasing progressively the inlet velocity is used to solve the problem (12). The non-linearity due to the convection term is treated thanks to the Newton method. At each step of the Newton loop, a multi-frontal Gauss LU factorization [34], implemented in the package UMFPACK [35], permits to solve the linearized discrete problem. The numerical method has been implemented in the framework of the open source finite element software FreeFEM++ [36]. Finally, minor changes have been provided here in comparison to the original method described in [30]. Those are the following:

- As it can be seen in (12), both the symmetrical and antisymmetrical parts of the convection term have been kept, and thus convection is discretized in a natural way (the symmetrical part of the convection was removed in [30] for the purpose of the analysis).
- The Taylor–Hood element with a quadratic interpolation of the velocity [24] has been chosen instead of the $\mathbb{P}_2/\mathbb{P}_1/\mathbb{P}_0$ element suggested in [30], so as to allow a better approximation of the pressure and of the shear stress. Let us emphasize that for this element, the grad–div stabilization is strictly necessary so that the problem admits a solution [30, Remark (1) p.60].[1] As a result, we put $\lambda > 0$.
- Mesh refinement may be carried out after the first step of the continuation loop, to enhance the precision of the computation near the bump. A variable metric/Delaunay meshing algorithm based on the Hessian of the velocity/pressure, with a constraint of mesh isotropy, has been used for this purpose [36].

In the case of the Double Deck equations, the matching condition at infinity (6) is implemented simply as a Dirichlet boundary condition on the left side (inlet) and upper side of the domain, *i.e.*

$$u = v = 0 \text{ on } y = y_w,\ u = y \text{ when } x = 0, \text{ and } u = y \text{ when } y = Y_{\mathrm{MAX}}, \tag{13}$$

where Y_{MAX} denotes the height of the computational domain. Note that this is only an approximation of (6). This is valid if the bump is sufficiently far away from the inlet and if Y_{MAX} is sufficiently large. For the examples presented below in Section 4, the bump is typically at a distance $x = 5$ away from the inlet, and the value of Y_{MAX} is 40, which should ensure a good approximation of the exact condition (6).

[1] A straightforward adaptation of Lemmas 1 and 3 in [30] also shows that the discrete problem for RNS/P admits a solution with any kind of inf–sup stable element for Stokes and a grad–div stabilization.

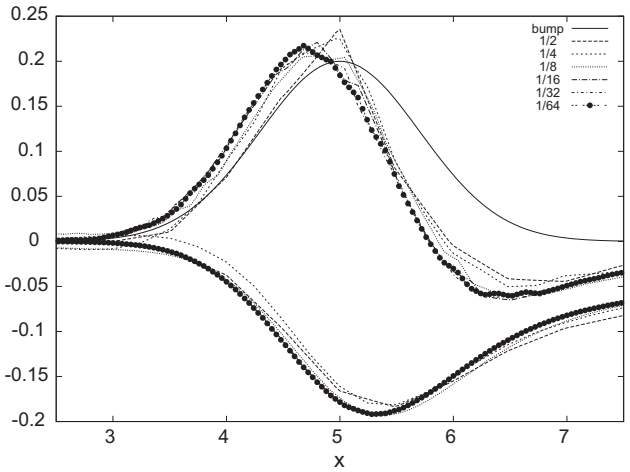

Fig. 2. The gaussian bump of height $\alpha = 0.2$, the perturbation (to emphasize the effect) of the skin friction ($\tau - 1$) and the pressure, in the Finite Element case (FE). Influence of the size of the smaller elements (1/2, 1/4, 1/8, 1/16, 1/32, and 1/64, the three last values lead to nearly superposed curves).

Table 1
Convergence of pressure and wall shear stress as a function of the mesh size, the error is relative to the 1/64 case which is taken as reference.

hmin	Nodes	Triangles	Error p	Error τ
1/2	893	1669	4.63E−002	5.43E−002
1/4	2218	4217	6.89E−002	4.44E−002
1/8	4301	8213	3.60E−002	2.78E−002
1/16	5718	10990	4.10E−003	1.09E−002
1/32	10770	20982	5.00E−004	8.40E−003
1/64	30790	60800	0.00	0.00

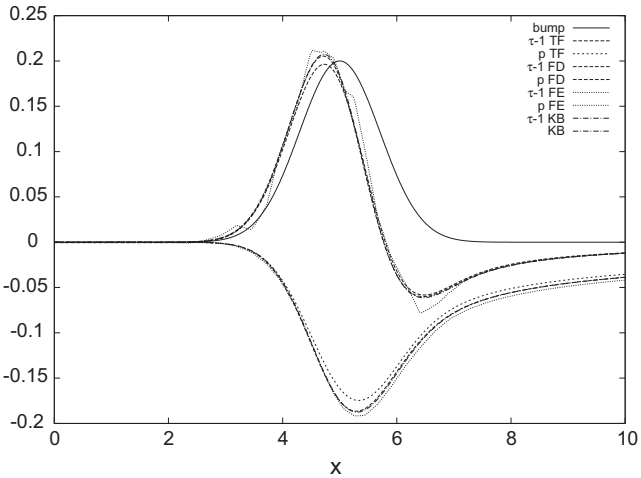

Fig. 3. The bump, the perturbation (to emphasize the effect) of the skin friction ($\tau - 1$) and the pressure, in the Double Deck case. The height of the bump is 0.2. Comparison of the (FD KB and FE), and linear analytical expression DD Eq. (7) for τ and (8) for p. The pressure and skin friction are nearly the same for the four methods. The results of KB and FD are superposed. The FE code increases a little the pressure drop. For the skin friction, the FE solution is a bit jagged. The linear solution differs slightly but it is due to the fact that 0.2 is not so small.

4. Numerical experiments

In these sections, we compute with the different methods the flow over a simple gaussian $y_w(x) = \alpha e^{-(x-5)^2}$ bump. For the finite differences method the numerical parameters are: $\Delta x = 0.0125$ and $\Delta y = 0.005$ whereas the KB uses $\Delta x = 0.025$ and $\Delta y = 0.06$, the size of the domain is 6 or more, leading to *ca.* respectively 1,500,000 and 60,000 degrees of freedom.

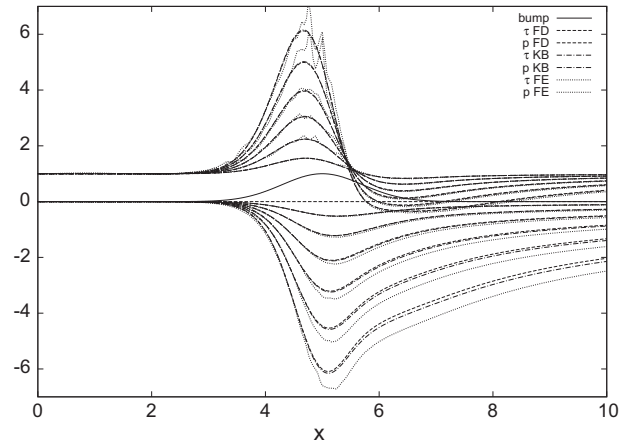

Fig. 4. The bump, the skin friction (τ) and the pressure as the height of the bump increases (size of the bump from 0.5, 1.0, 1.5, and 2.0) in the Double Deck case. Comparison of FD, KB and FE. There is a very small difference between FD and KB, and a noticeable between those two and FE. It is likely that we observe the effect of the FLARE approximation.

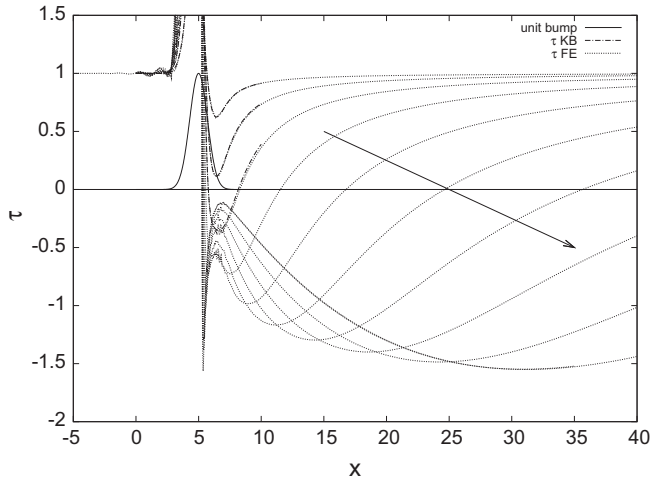

Fig. 5. Reduced skin friction τ in the Double Deck case DD for large height of the bump. FEM: $\alpha = 1, 2, 3, 4, 5, 6, 7, 8, 9, 10$ and KB $\alpha = 1, 2, 3$. Arrow in the direction of increasing α. KB fails for $\alpha > 3.5$, for this value, a sharp kink begins to appear and a maximum of the negative skin friction appears as well (note the small oscillation before the fast increase of shear stress which is a coarse mesh effect).

For the finite element method, the mesh is an unstructured mesh generated automatically by FreeFEM++, with mesh refinement near the bump. The size of the mesh after refinement can vary slightly from one example to another. To give an idea, for the computation presented Fig. 3, the mesh, after refinement, is made of 3542 vertices, and 6824 triangles. This results into 31356 degrees of freedom, since the Taylor–Hood element is used. As a consequence, the finite element approximation needs less degrees of freedom than FD and KB methods to reach approximatively the same precision. This is due in particular to the nature of the interpolation in the finite element method (piecewise linear and quadratic, as opposed to punctual values in FD/KB). Despite of this, the FE method is quite time consuming in comparison to FD and KB, since the methods are of very different nature (see the discussion Section 5). The number of continuation iterations is 5. At each continuation iteration, Newton loops are carried out until convergence (with a convergence criterion of 10^{-10} on the norm of the velocity). The stabilization parameter λ is fixed to 1 and its value is motivated by the numerical studies in [30]. See on Fig. 2 examples of pressure and perturbation of skin friction from the basic state with different mesh sizes, which show that the method converges when the mesh size is reduced. On Table 1, we display the estimated error (using the finer mesh as reference) for pressure and shear computed as follows:

$$Error = \sqrt{\int_0^L (\phi(x) - \phi_{\mathrm{ref}}(x))^2 dx} \text{ where } \phi \text{ stands for } p \text{ and } \tau.$$

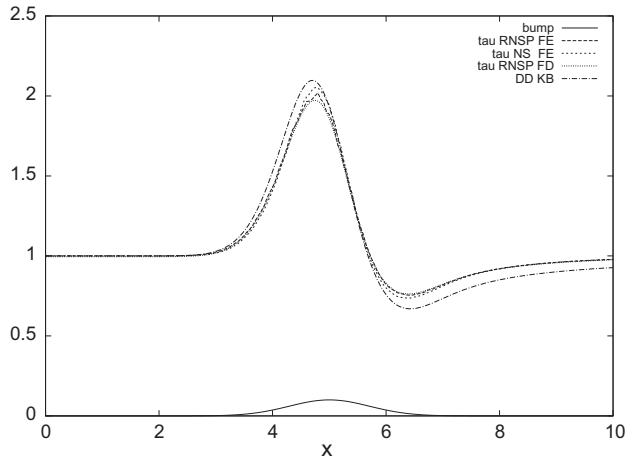

Fig. 6. Skin friction on the bump of height $\alpha = 0.1$, comparison of the RNSP (FD and FEM), NS (FEM), and DD (KB) for Reynolds $Re = 750$. In Double Deck scales the height of the bump is $\alpha Re^{1/3} = 0.91$. The RSNP results are superposed for FD and FE. The Navier–Stokes solution is a little bit different: the RNSP underestimates the maximum. The Double Deck over estimates the skin friction.

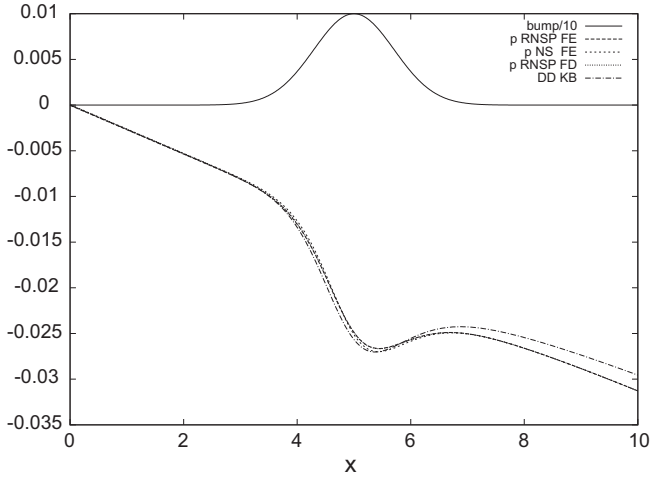

Fig. 7. Pressure on the bump, comparison of the RNSP (FD and FEM), NS (FEM), and DD (KB), $Re = 750$. For the latter the basic Poiseuille pressure has been added so that $-2x/Re + Re^{-2/3}p$ is plotted. The zero value of the pressure has been put at the origin. The RNSP solutions and NS solution are superposed. The Double Deck solution differs a bit in downstream part of the bump.

4.1. Double Deck examples

On Fig. 3 we compare the linearized analytical solution of the Double Deck equations ((7) for τ and (8) for p), the finite differences, the Keller Box and the finite elements numerical solutions for $\alpha = 0.2$. We draw the perturbation of skin friction $\tau - U_0'$ and the perturbation of pressure. The fact that the skin friction is extremal before the crest of the bump and decreases after the crest is a classical observation. A pressure drop is associated, the minimum of pressure is after the crest of the bump. The pressure is nearly the same for the four methods, except the FE which increases a bit the pressure drop. The Keller Box method and the finite difference method give superposed results. The FE solution is a bit jagged for the skin friction obtained by derivation of the velocity due to the choice of the elements (continuous interpolation with Lagrange elements). As $\alpha = 0.2$ is not so small, there is a small difference between the three numerical non linear resolutions and the linear resolution by Fourier transform.

On Fig. 4, we increase the height α of the bump and explore the nonlinearities of the Double Deck problem. We even have separation of the flow (τ becomes negative after the bump crest). We compare finite differences, Keller Box and finite elements. The two first are again very similar, though not exactly the same. The pressure is a bit different for the FE computation. The differences in this part are maybe due to the FLARE approximation (put $u = 0$ when $u < 0$) as the implementation is slightly different in KB and FD, and as there is no such approximation in FE.

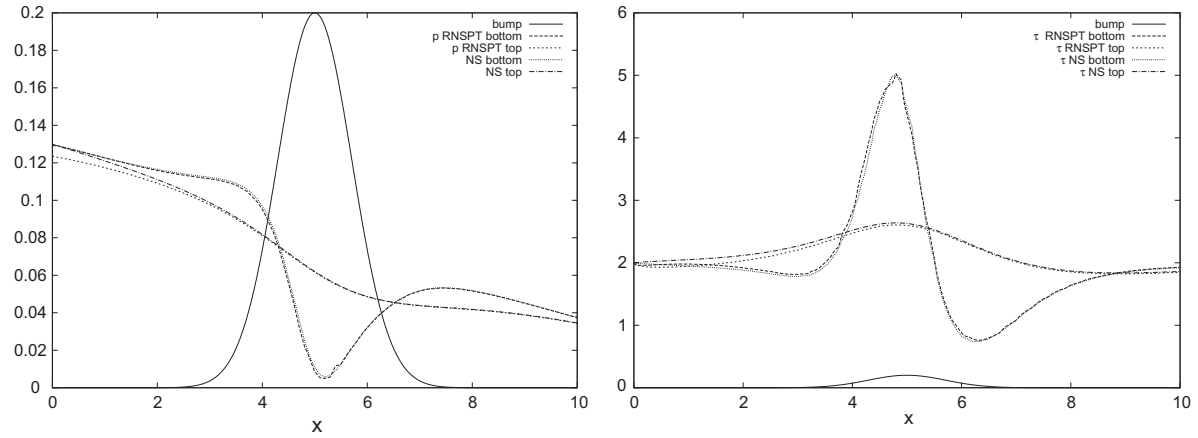

Fig. 8. Comparing NS and RNSP with transverse effects. Flat upper wall, and bumpy lower wall. Observe the upstream influence of the Skin friction and of the pressure.

On Fig. 5, we increase much more the height α of the bump and explore the nonlinearities of the Double Deck problem for large bumps. Up to now, the finite differences resolutions were done with the FLARE simplification, which is unnecessary with the new finite element method (see [30]). So the reverse flow is more accurately computed. We observed previously that the skin friction is extremal before the crest, and decreases after. It may then be negative (for $\alpha \gtrsim 2.22$). When it is negative, it means that we have separation and there is a bulb of recirculation after the bump. For moderate values of α (in fact $\alpha \lesssim 3$), the skin friction becomes negative, reaches a minimum and it increases gently after. It becomes positive again, and then asymptotically goes to the undisturbed initial value. When α is more increased, after $\alpha \simeq 3$, the behavior of the skin friction changes. The skin friction becomes negative but it presents a flat part. Then, for large α a kink appears; after this minimum, the skin friction increases again. But it does not become positive, it reaches an extremum. Then it decreases again, it reaches a minimum and increases again gently, passes 0 and goes asymptotically to 1. The advantage of the finite element method is then clear as it allows large bump size. It is then better than the FD and KB which allow to compute a smaller separation bulb (associated to a smaller bump).

Recently [37] has obtained very similar results for the skin friction in different asymptotic Double Deck case corresponding to a wall jet flow encountering a bump. Similar features are observed for the behavior of the skin friction in the reverse flow region in case of large α. He used a numerical technique based on a finite-difference technique in the streamwise direction and Chebyshev collocation in the normal direction. So Chebyshev and finite elements give better results than finite differences or Keller Box which fail for $\alpha \gtrsim 3.5$.

4.2. RNSP example

Those preceding comparisons at Double Deck scales enabled us to validate the numerical method. We now compare the different asymptotic models and Navier–Stokes itself. So, on Fig. 6 we draw the skin friction for a value of $\alpha = 0.1$, and on Fig. 7 we draw the pressure (the zero value of the pressure has been put at the origin). We draw this for the asymptotic models (Double Deck Keller Box and RNS/P finite differences and finite elements) and for Navier–Stokes (finite elements) as well.

Note that the value of the height of the bump in the DD scale must be multiplied by $Re^{1/3}$ due to the change of scale. Note as well that the pressure of Double Deck is multiplied by $Re^{-2/3}$ and that the basic Poiseuille pressure has been added to the Double Deck pressure solution so that $-2x/Re + Re^{-2/3}p$ is plotted.

The results of all the models are very similar, even for this moderate value of the Reynolds number ($Re = 750$). We point out here that we choose the definition of the Reynolds number to have a unit slope at the wall. But constructed with the maximum value of the velocity the Reynolds is $R_m = Re/4$ and constructed with the average value of the velocity the Reynolds is only $R_a = Re/6$. So even for a rather small Reynolds the result of the asymptotic methods are very similar to Navier–Stokes.

5. Discussion and perspectives

We presented and cross-compared different numerical methods to compute the laminar steady viscous flow between two plates with symmetrical indentation. Of course, the Navier–Stokes numerical effort in those configurations is nowadays not very strong for moderate *Re*. But here, we presented equations which break the elliptic character of steady Navier–Stokes, those equations are parabolic.

We have an asymptotic hierarchy: first at infinite Reynolds number, we have the Double Deck description; in fact this description is included (see [25]) in the Reduced Navier–Stokes asymptotic description, which is itself included in the Navier–Stokes equations. The interest of asymptotical models is that they focus on the more important terms in the equations: they show that the most important terms are the longitudinal convection and the transverse diffusion, and also that the pressure can be considered approximatively constant in every transverse section.

We validated the different algorithms: two finite difference methods [22,20] and a finite element method issued from [30]. The interest of the finite element method is clearly that it allows to get rid of the FLARE approximation used in the finite differences marching methods. So, we presented original examples of massive separation after a large bump. A drawback of the finite element method is that it is not so much faster than the complete finite element Navier–Stokes resolution (see [30]), and this point is object of current research work. At the opposite, the finite differences marching methods are very fast as they are marching in x, and they are enough precise to tackle with moderate separation bulbs. The comparison with the FE method shows that the FLARE approximation is in fact enough precise, validating the approximation.

Interestingly enough, our implementation allows us to play with the terms, for example we can reintroduce part of the transverse equation from (1), for instance we reintroduce only:

$$u\frac{\partial v}{\partial x}+v\frac{\partial v}{\partial y}=-\frac{\partial p}{\partial y} \tag{14}$$

which is nearly (9) at large Reynolds. Then as expected from linear theory of flow in non symmetrical channels [17], there is an upstream effect. This means that upstream the bump, the skin friction and the velocity are disturbed (breaking the parabolicity). We can see this on Fig. 8 where RNSP with the transverse equation (14) are solved and compared to Navier–Stokes. This opportunity to remove terms in Navier–Stokes is very promising and opens the possibility to a lot of comparisons of asymptotic models at large *Re* versus full Navier–Stokes.

Acknowledgments

We acknowledge G. Barrenechea, R. Araya, X. Pelorson, A. van Hirtum, N. Henrich, T. Chacón, U. Razafison, J. Sainte Marie for some helpful discussions and comments. Part of this work has been realized during first author's postdoctoral stage at Projet REO, INRIA CRI Paris-Rocquencourt and Laboratoire Jacques-Louis Lions (UPMC).

References

[1] S.A. Berger, L-D Jou, Flows in stenotic vessels, Ann. Rev. Fluid Mech. 32 (2000) 347–382.
[2] T.J. Pedley, The Fluid Mechanics of Large Blood Vessels, Cambridge University Press, 1980.
[3] T.J. Pedley, Perspectives in Fluid Dynamics, in: G.K. Batchelor, H.K. Moffatt, M.G. Worster (Eds.), (chapter 3). Blood Flow in Arteries and Veins, Cambridge University Press, 2000, pp. 105–158.
[4] X. Pelorson, A. Hirschberg, A.-P.-J. Wijnands, H. Bailliet, Description of the flow through in-vitro models of the glottis during phonation, Acta Acustica 3 (1995) 191–202.
[5] B. Shome, L.-P. Wang, M.-H. Santare, A.-K. Prasad, A.-Z. Szeri, D. Roberts, Modeling of airflow in the pharynx with application to sleep apnea, J. Biom. Eng. 120 (1998) 416–422.
[6] R.-C. Scherer, D. Shinwari, K.-J. De Witt, C. Zhang, B.-R. Kucinschi, A.-A. Afjeh, Intraglottal pressure profiles for a symmetric and oblique glottis with a divergence angle of 10 degrees, J. Acoust. Soc. Am. 109 (2001) 1616–1630.
[7] M.P. Païdoussis, Fluid-Structure Interactions. Volume 2. Slender Structures and Axial Flow, Elsevier, 2000.
[8] R. Glowinski, O. Pironneau, Finite element methods for Navier–Stokes equations, Ann. Rev. Fluid Mech. 24 (1992) 167–204.
[9] S. Turek, Efficient Solvers for Incompressible Flow Problems. An Algorithmic and Computational Approach, Springer, 1999.
[10] P. M Gresho, R.L. Sani, Incompressible Flow and the Finite Element Method, John Wiley & Sons, 2000.
[11] O.E. Zienkiewicz, R.L. Taylor, P. Nithiarasu, The Finite Element Method for Fluid Dynamics, sixth ed., Butterworth, Heinemann, 2005.
[12] M. Van Dyke, Perturbation Methods in Fluid Mechanics, Parabolic Press, 1975.
[13] L. Prandtl, Motion of fluids with little viscosity/ vier abhandlungen zur hydrdynamik und aerodynamik göttingen 1927, 1928. NACA report 452.
[14] H. Schlichting, Boundary-layer Theory, seventh ed., McGraw-Hill Publishing Company, New-York, 1987.
[15] H. Schlichting, K. Gersten, Boundary-layer Theory, eighth ed., Springer, 2000.
[16] J. Cousteix, J. Mauss, Asymptotic Analysis and Boundary Layers, Springer, 2007.
[17] I.J. Sobey, Introduction to Interactive Boundary Layer Theory, Oxford University Press, Applied and Engineering Mathematics, 2000.
[18] V.V. Sychev, A.I. Ruban, V.V. Sychev, G.L. Korolev, Asymptotic Theory of Separated Flows, Cambridge University Press, 1998.
[19] H. Steinrück, Asymptotic Methods in Fluid Mechanics: Survey and Recent Advances. Cism Courses and Lectures, Springer, 2010.
[20] H.B. Keller, Numerical methods in boundary layer theory, Ann. Rev. Fluid Mech. 10 (1978) 417–433.
[21] G.L. Korolev, J.S.B. Gajjar, A.I. Ruban, Once again on the supersonic flow separation near a corner, J. Fluid Mech. 463 (2002) 173–199.
[22] P.-Y. Lagrée, E. Berger, M. Deverge, C. Vilain, A. Hirschberg, Characterization of the pressure drop in a 2D symmetrical pipe: some asymptotical, numerical and experimental comparisons, ZAMM Z. Angew. Math. Mech. 85 (2) (2005) 141–146.
[23] F.T. Smith, Flow through constricted or dilated pipes and channels Parts 1 and 2, Q. J. Mech. Appl. Math. 29 (1976) 232–253. & 254–265.
[24] A. Ern, J.-L. Guermond, Theory and Practice of Finite Elements, Springer-Verlag, 2004.
[25] P.-Y. Lagrée, S. Lorthois, The RNS/Prandtl equations and their link with other asymptotic descriptions: application to the wall shear stress scaling in a constricted pipe, Int. J. Eng. Sci. 43 (2005) 352–378.
[26] A. Van Hirtum, X. Pelorson, P.-Y. Lagrée, In vitro validation of some flow assumptions for the prediction of the pressure distribution during obstructive sleep apnea, Med. Biol. Eng. Comp. 43 (2005) 162–171.
[27] P.-Y. Lagrée, A. Van Hirtum, X. Pelorson, Asymmetrical effects in a 2D stenosis, Eur. J. Mech. B 26 (2007) 83–92.
[28] F. Chouly, A. Van Hirtum, P.-Y. Lagrée, X. Pelorson, Y. Payan, Numerical and experimental study of expiratory flow in the case of major upper airway obstructions with fluid-structure interaction, J. Fluid. Struct. 24 (2008) 250–269.
[29] P. Bradshaw, T. Cebecci, J.H. Whitelaw, Engineering Calculation Methods for Turbulent Flow, Academic Press, 1981.
[30] G.R. Barrenechea, F. Chouly, A finite element method for the resolution of the Reduced Navier–Stokes/Prandtl equations, ZAMM Z. Angew. Math. Mech. 89 (1) (2009) 54–68.

[31] P. Azérad, F. Guillén, Mathematical justification of the hydrostatic approximation in the primitive equations of geophysical fluid dynamics, SIAM J. Math. Anal. 33 (4) (2001) 847–859.
[32] R. Peyret, T.D. Taylor, Computational Methods for Fluid Flow. Springer Series in Computational Physics, Springer-Verlag, 1983.
[33] T.-A. Reyhner, Flügge-Lotz, The interaction of a shockwave with a laminar boundary layer, Int. J. Non-Linear Mech. 3 (1968) 173–199.
[34] T.A. Davis, I.S. Duff, A combined unifrontal/multifrontal method for unsymmetric sparse matrices, Technical Report 20, CISE, University of Florida, 1999.
[35] T.A. Davis, Algorithm 832: UMFPACK V4.3- an unsymmetric-pattern multifrontal method, ACM Trans. Math. Software 30 (2004) 196–199.
[36] F. Hecht, O. Pironneau, A. Le Hyaric, and K. Ohtsuka, Freefem++ 2.16-1 documentation, 2007. Webpage: http://www.freefem.org/ff++.
[37] R. Yapalparvi, Double-deck structure revisited, Eur. J. Mech. – B/Fluids 31 (0) (2012) 53–70.